Controlling the molecular diffusion in MOFs with the acidity of monocarboxylate modulators

Isabel Abánades Lázaro[a]‡*, *Catalin Popescu*[b] *and Francisco G. Cirujano*[a]‡*

[a] Instituto de Ciencia Molecular (ICMol), Universitat de València, Catedrático José Beltrán Martínez nº 2, 46980 Paterna, Valencia, Spain.

[b] ALBA Synchrotron, Carrer de la Llum 2-26 08290 Cerdanyola del Vallès, Barcelona, Spain

‡These authors contributed equally.

Table of contents

S1. General Experimental Remarks

Powder X-Ray Diffraction (PXRD): PXRD patterns were collected in a PANalytical X'Pert PRO diffractometer using copper radiation (Cu Kα = 1.5418 Å) with an X'Celerator detector, operating at 40 mA and 45 kV. Profiles were collected in the 3° < 2θ < 40° range with a step size of 0.017°. (University of Valencia).

High angular resolution experiments of Synchrotron XRD were performed on the powder diffraction end station of the MSPD beamline[1] at the ALBA Synchrotron in Barcelona.

The SXRD patterns were collected in the high resolution multianalyzer detector (MAD) set-up with 13 keV beam energy (λ =0.9531 Å). The samples were contained in quartz capillaries of 0.7 mm diameter, which were rotating during collection time.

Thermogravimetric Analysis (TGA): were carried out with a Mettler Toledo TGA/SDTA 851 apparatus between 25 and 800 °C under ambient conditions (10 °C·min^{-1} scan rate and an air flow of 9 mL·min−1). (University of Valencia)

Nuclear Magnetic Resonance Spectroscopy (NMR): NMR spectra were recorded on either a Bruker AVIII 300 MHz spectrometer and referenced to residual solvent peaks. (University of Valencia)

Gas Uptake: N_2 adsorption isotherms were carried out at 77 K on a with a Micromeritics 3Flex gas sorption analyser. Samples were degassed under vacuum at 120 °C for 24 h in a Multisorb station prior to analysis. BET surface areas, micropore surface areas and external surface areas were calculated from the isotherms using the MicroActive operating software. The pore size distributions were calculated using NLDFT slit carbon pore model within the MicroActive software, applying a regularisation of 10^{-2} (University of Valencia)

Scanning Electron Microscopy (SEM) and single point energy-dispersive X-Ray analysis (EDX): particle morphologies, dimensions and mapping were studied with a Hitachi S-4800 scanning electron microscope at an accelerating voltage of 20 kV, over metalized samples with a mixture of gold and palladium during 90 seconds. (University of Valencia). ImageJ software was employed to analise the particle size distrubutions.

Fourier Transform Infrared Spectroscopy: IR spectra of solids were collected using a Shimadzu Fourier Transform Infrared Spectrometer, FTIR-8400S, fitted with a Diamond ATR unit. (University of Valencia)

S.2. Materials and Synthesis

All reagents unless otherwise stated were obtained from commercial sources and were used without further purification.

In 25 mL pyrex jars, $ZrCl_4$ (1 equivalent, 0.9 mmol, 237 mg) was dissolved in 5 mL of DMF. In a separate vial, BDC (1.5 equivalents, 1.35 mmol, 224 mg), was dissolved in 5 mL of DMF, to which 10 equivalents of modulator compared to BDC (15 compare to metal) were added (either 0.510 mL of FA, 1.033 mL of TFA or 1.648 g of BA). Upon complete dissolution by sonication, both solutions were mixed in a 25mL pyrex jar and placed in an oven at 120°C over 24 hours.

^{1}HNMR characterization: approximately 5 mg of MOF were digested in 0.6 mL of d^6-DMSO with 5 drops of D_2SO_4 by heating at 75°C and stirring until complete dissolution.

Activation: The precipitate was collected by centrifugation and washed with DMF (X2) and MeOH (X3) by dispersion/centrifugation cycles (4500rpm, 5 minues). Then, the samples were further activated with Soxhlet (boiling MeOH) over night and further dried with vacuum at 120°C during 24h.

S.3. Characterisation of UiO-66 modulated samples

S.3.1. Assessing MOFs crystallinity by PXRD patterns.

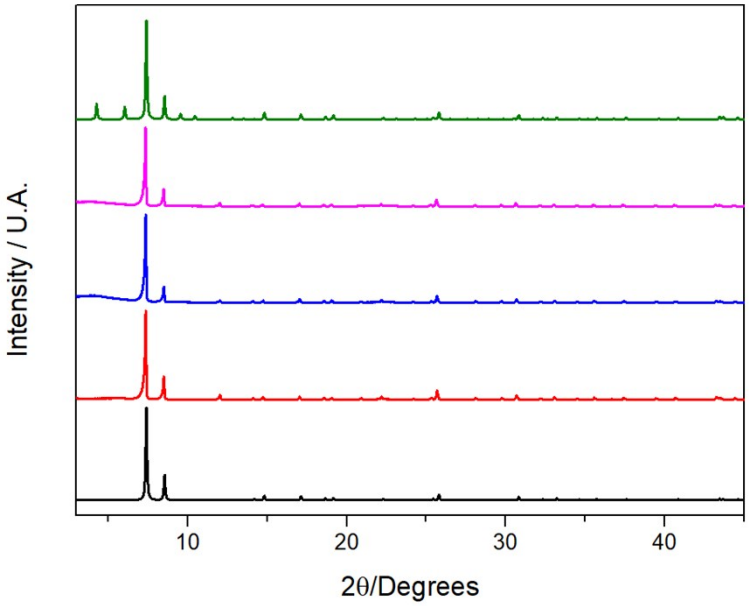

Figure S1: Stacked PXRD patterns of modulated UiO-66 synthesized compared to simulated pristine UiO-66 and defective missing cluster reo phase. (Black) simulated defect-free UiO-66, (red) FA@UiO-66, (blue) TFA@UiO-66, (pink) BA@UiO-66 and (green) simulated reo phase.

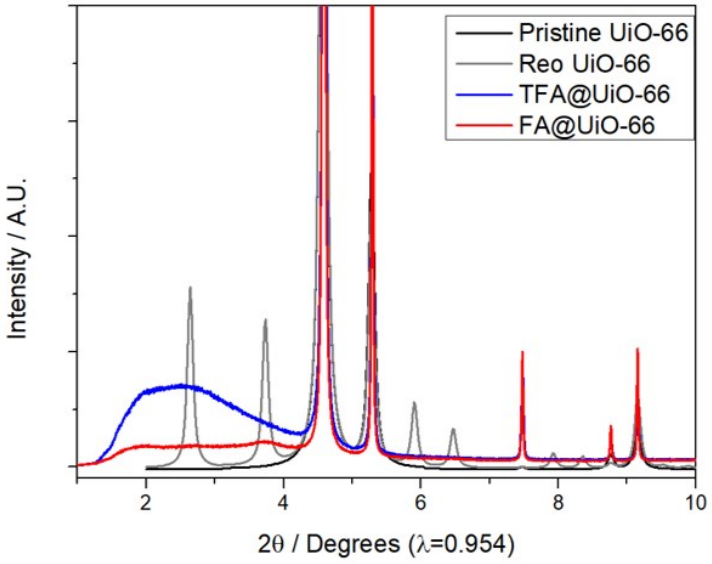

Figure S2: Compiled PXRD patterns of modulated UiO-66 synthesized compared to simulated pristine UiO-66 and defective missing cluster ***reo*** phase. Measured with synchrotron radiation.

S.3.2. Modulator content assessed by ^{1}HNMR

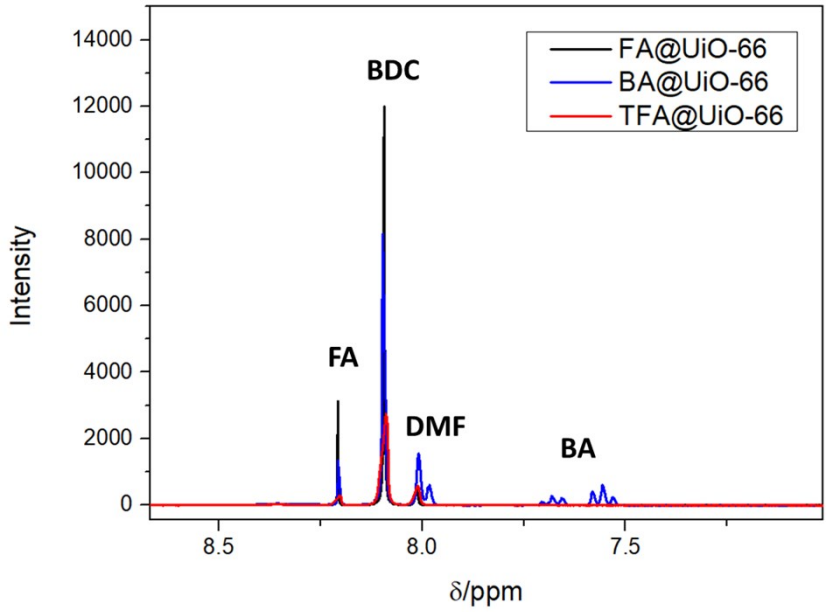

Figure S3: Amplification of the acid-digested d^{6}MSO ^{1}HNMR spectra of UiO-66 modulated samples, showing FA (either added or coming from the decomposition of DMF [2] and BA presence. Traces of DMF are also present in the samples, which are considered during the further determination of the composition by the combination of NMR and TGA techniques. Since TFA does not have protons, its content cannot be analysed by ^{1}HNMR alone.

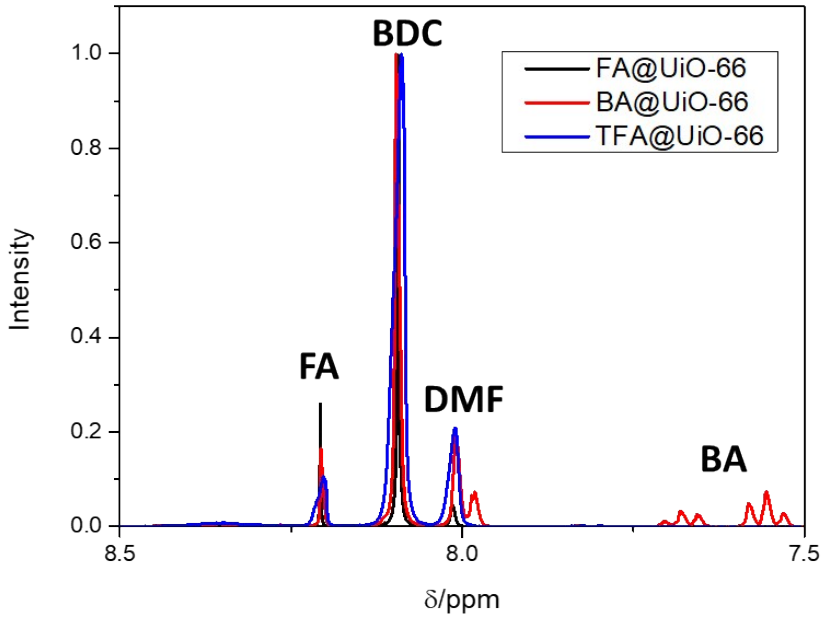

Figure S4: Amplification of the acid-digested d^{6}MSO ^{1}HNMR spectra of UiO-66 modulated samples (Normalised to BDC content).

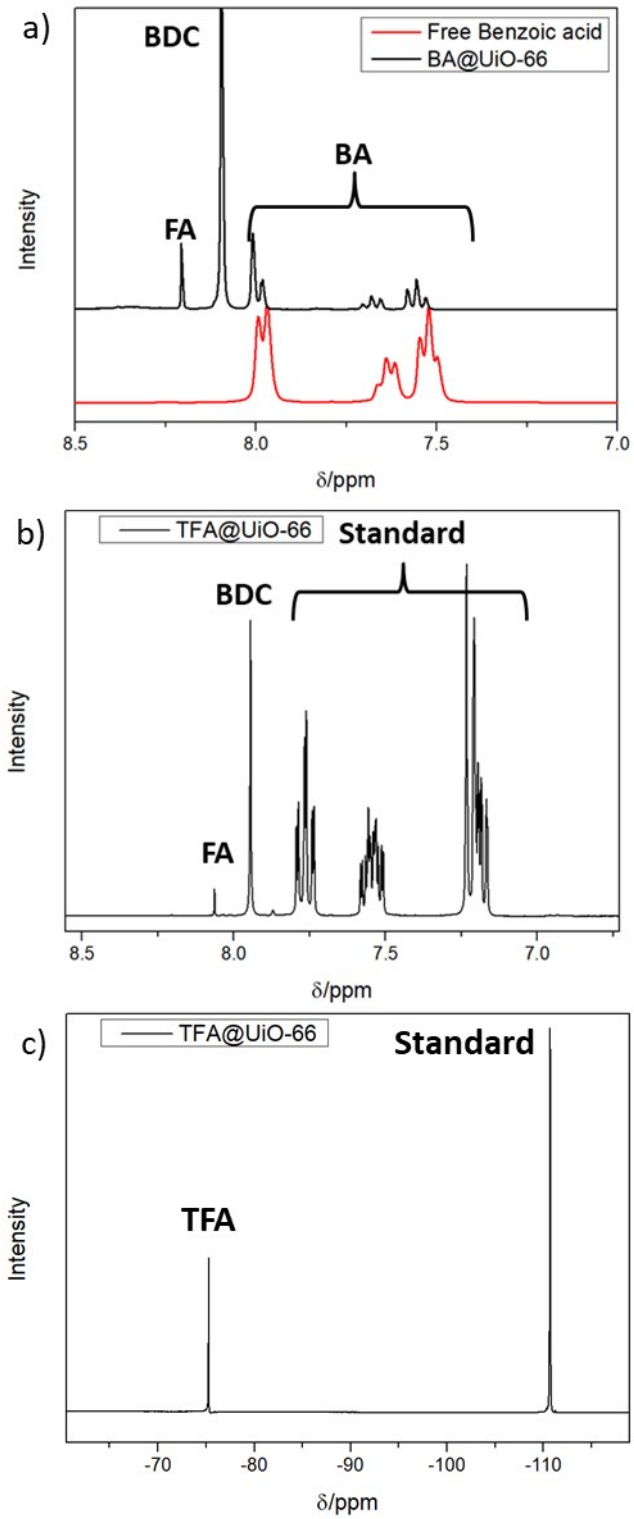

Figure S5: Amplification of the acid-digested d^{6}MSO ^{1}HNMR spectra of a) BA@UiO-66 compared to the spectra of free benzoic acid (under the same sample digestion conditions), b) TFA@UiO-66 with internal standard and c) ^{13}FNMR TFA@UiO-66 with internal standard.

Table S1: Tabulated ratio (*i.e.* $mod\,ratio = \frac{mod}{bdc}$), mole per cent (*mol%* $= \frac{mod}{mod + bdc} * 100$) of modulators and total modulator per cent, corresponding to the added modulator and co-incorporated FA, calculated by ^{1}HNMR of acid-digested d^{6}MSO samples.

Sample	**MOD/BDC**	**FA/BDC**	**MOD%**	**TOTAL MOD%**	DMF
FA@UiO-66	0.292	0.292	22.624	22.624	0.289
TFA@UiO-66	0.423*	0.179	29.73*	37.578	0.596
BA@UiO-66	0.192	0.215	16.129	28.962	0.566

*Note that since TFA has no protons, a combination of fluor and proton NMR has been used to calculate the molar ratio between modulator and linker (represented in Figure S5). [2] FA (δ 8.2 pp) was calculated based on the ratio between its integral (1H) and the linker's integral (δ 8.1 ppm, 4H). BA was calculated based on the relation between its integral at δ 7.6 ppm (1H) and the linker's integral. Note that due to acidification minor shifting of the peaks can occur.

See section S.3.4 for the assessment of DMF defect-compensating ligands or obstructed in the pores)

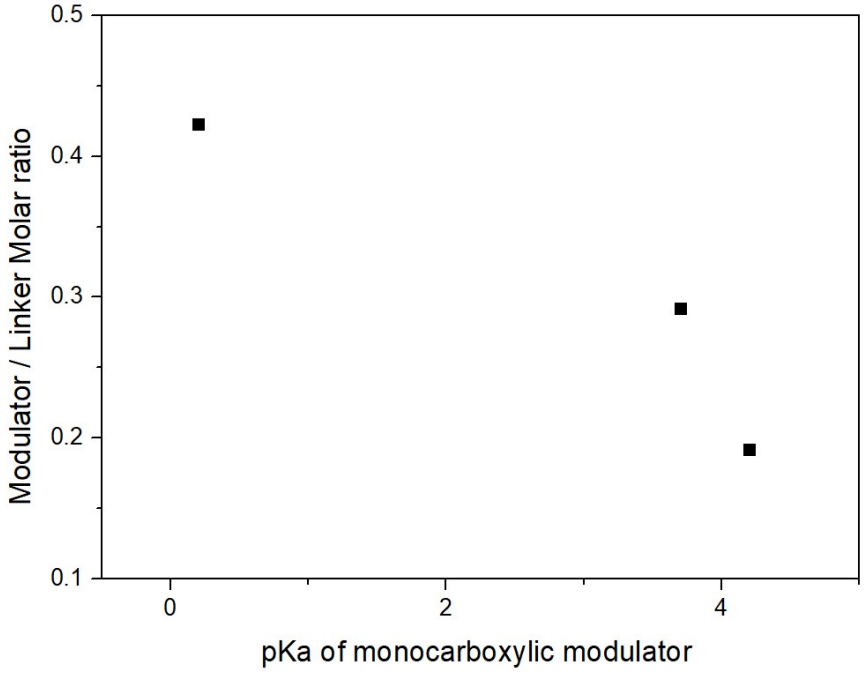

Figure S6: Representation of the **modulator/linker ratio** (added modulator) of the modulated samples as a function of the pK_a of the added modulator.

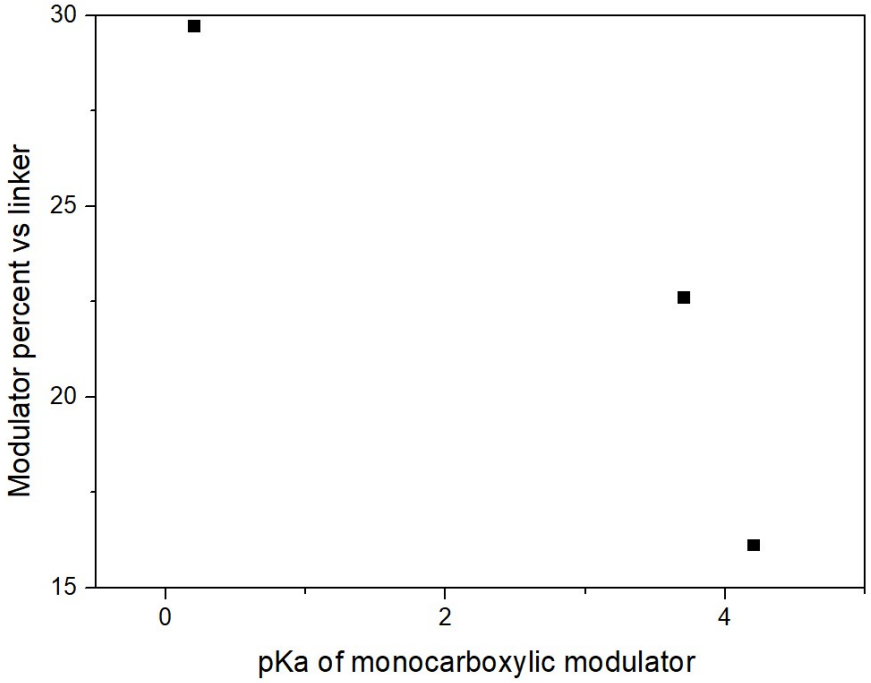

Figure S7: Representation of the **modulator mole per cent** (added modulator) of the modulated samples as a function of the pK_a of the added modulator.

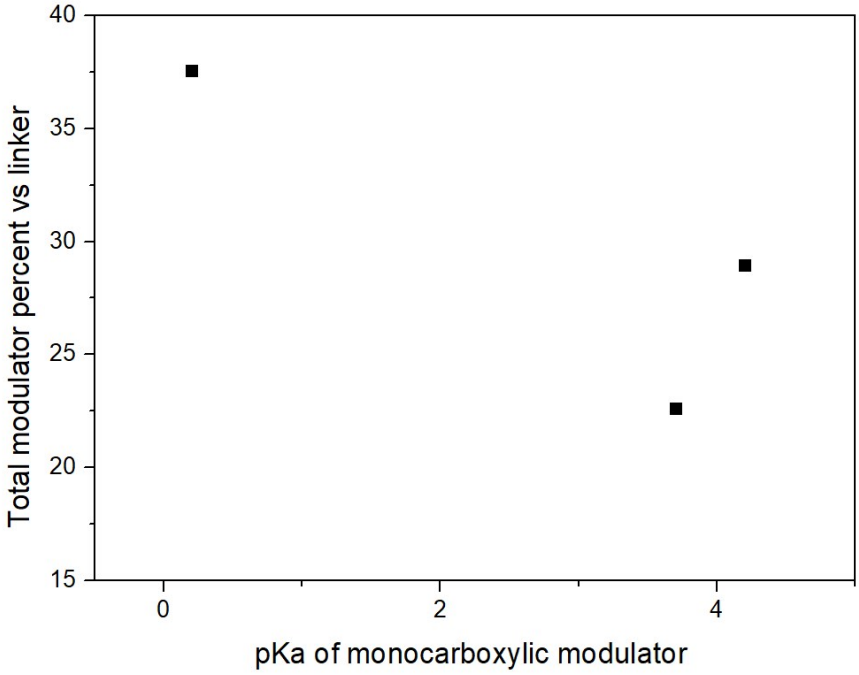

Figure S8: Representation of the **total modulator mole per cent** (added modulator and co-incorporated FA) of the modulated samples as a function of the pK_a of the added modulator,

showing that TFA (pK_a 0.2) and BA (pK_a 4.2) have a higher number of total modulator than FA due to the co-incorporation of the last, coming from the decomposition of DMF during synthesis.

S.3.3. Assessing modulators attachment by FT-IR profiles

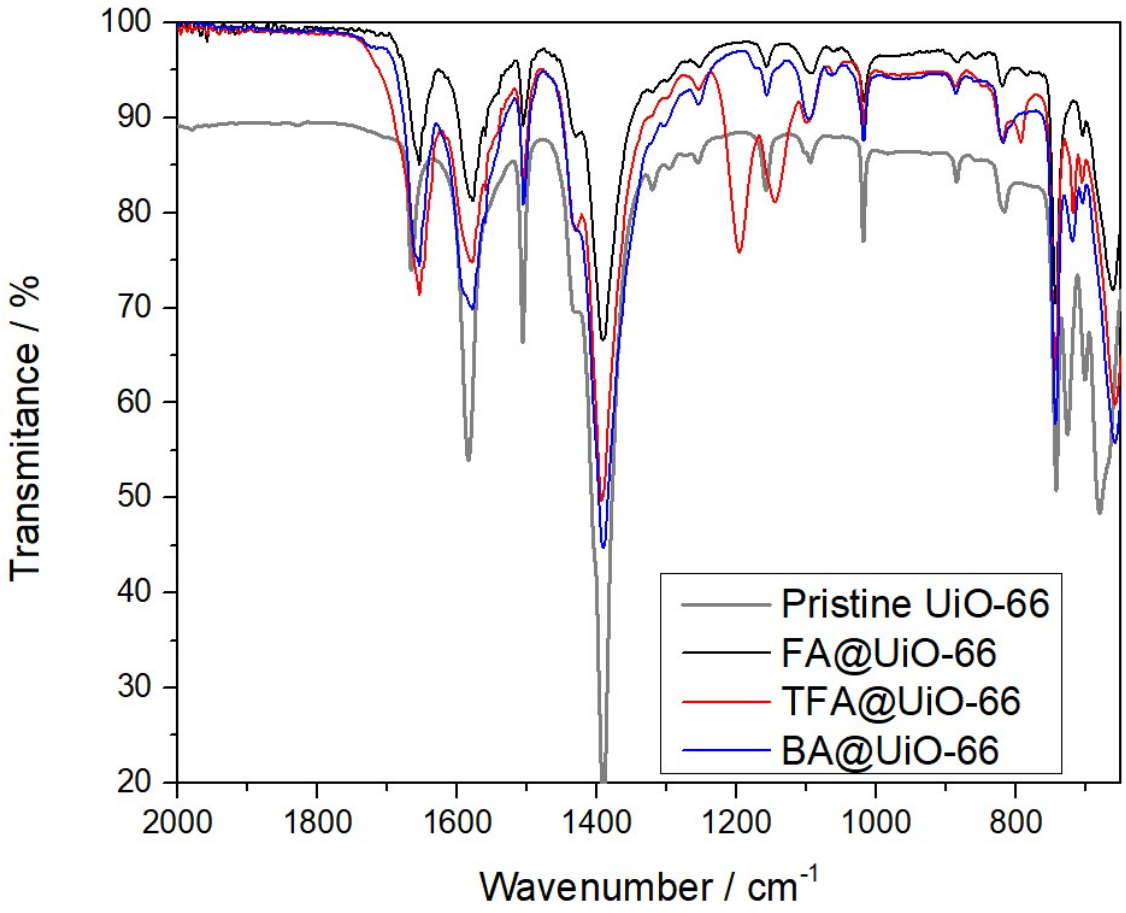

Figure S9: FT-IR of modulated UiO-66, showing shifting in the metal vibration bands (ca. 700 cm^{-1}), and no new signals in the carboxylate region (ca. 1800-1600 cm^{-1}) indicating attachment to the metal clusters.

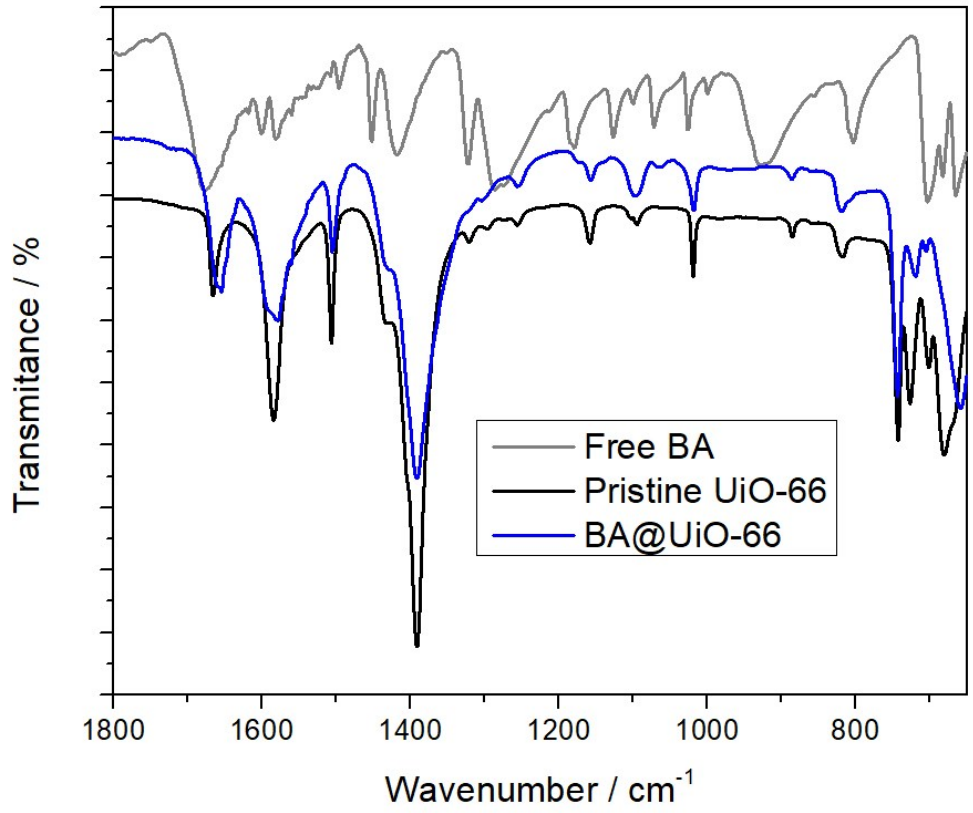

Figure S10: FT-IR of modulated UiO-66 compared to free BA, showing shifting in the metal vibration bands (ca. 700 cm^{-1}), and no new signals in the carboxylate region (ca. 1700 cm^{-1}) indicating attachment to the metal clusters.

S.3.4. Assessing MOFs composition and defectivity by TGA

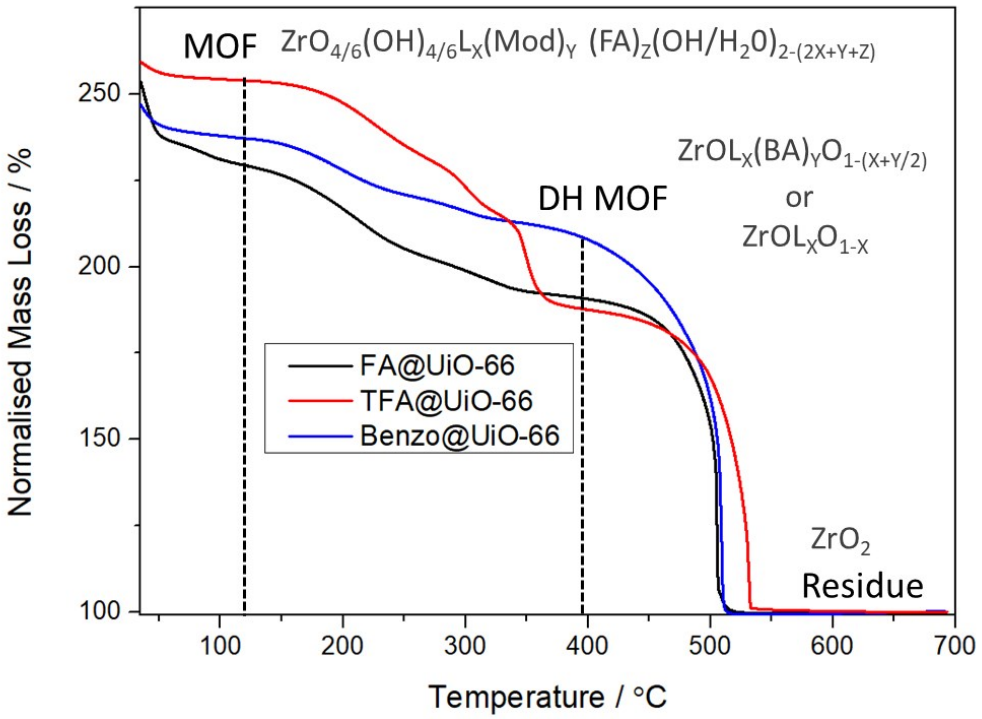

Figure S11: Thermal decomposition profiles of modulated UiO-66, normalizing the metal residues to 100%. DH: Dehydrated

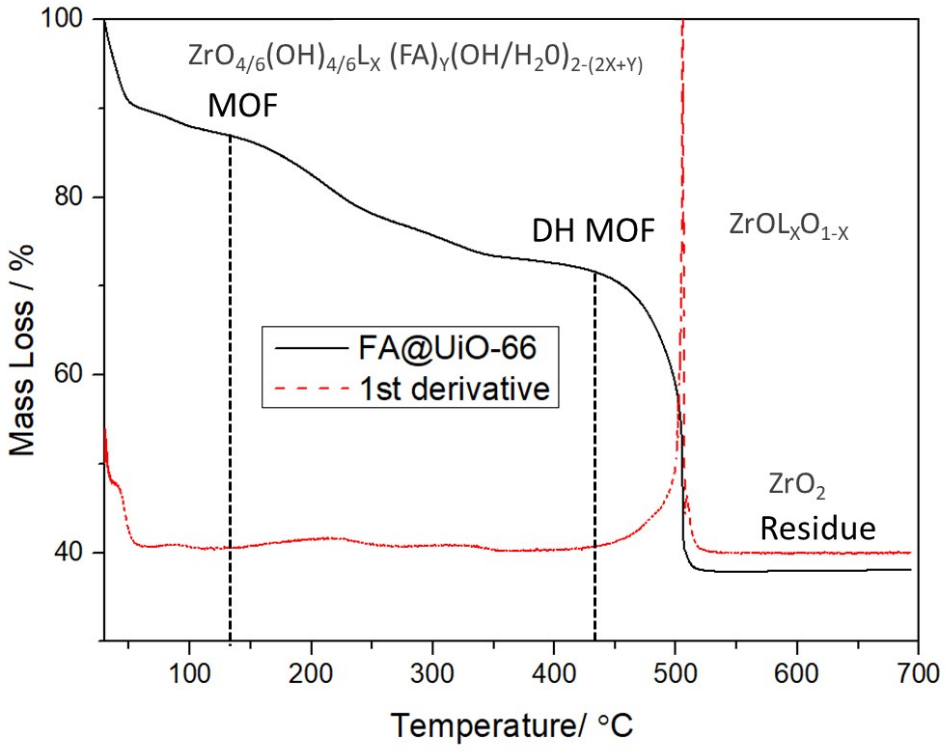

Figure S12: Thermal decomposition profile of FA@UiO-66 normalizing the start of the decomposition profile to 100%, alongside with its proposed structure.

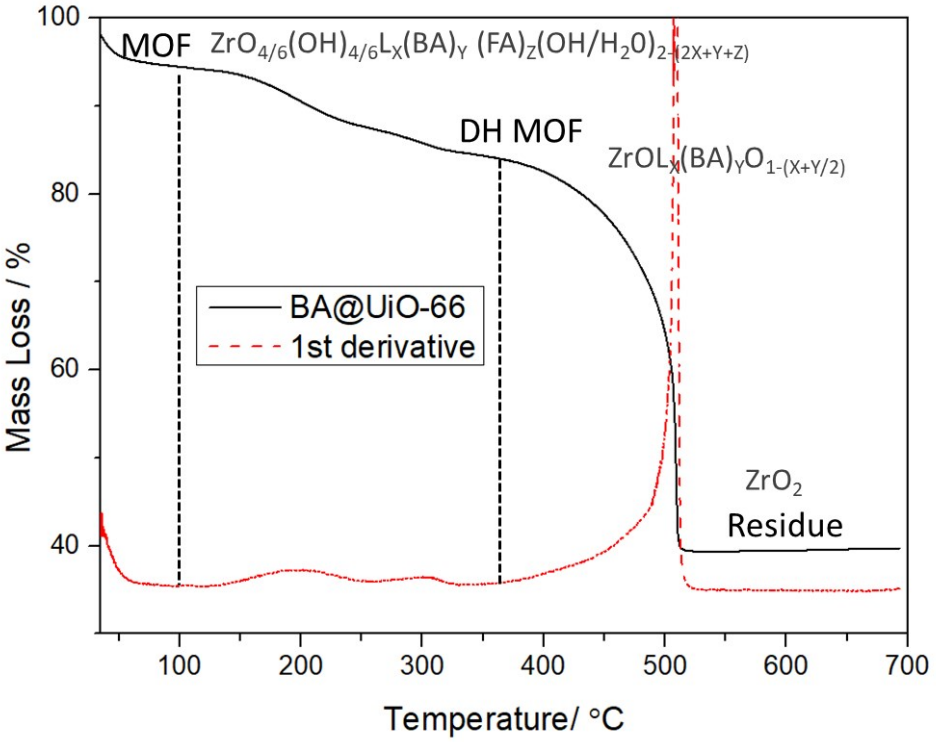

Figure S13: Thermal decomposition profile of BA@UiO-66 normalizing the start of the decomposition profile to 100%, alongside with its proposed structure.

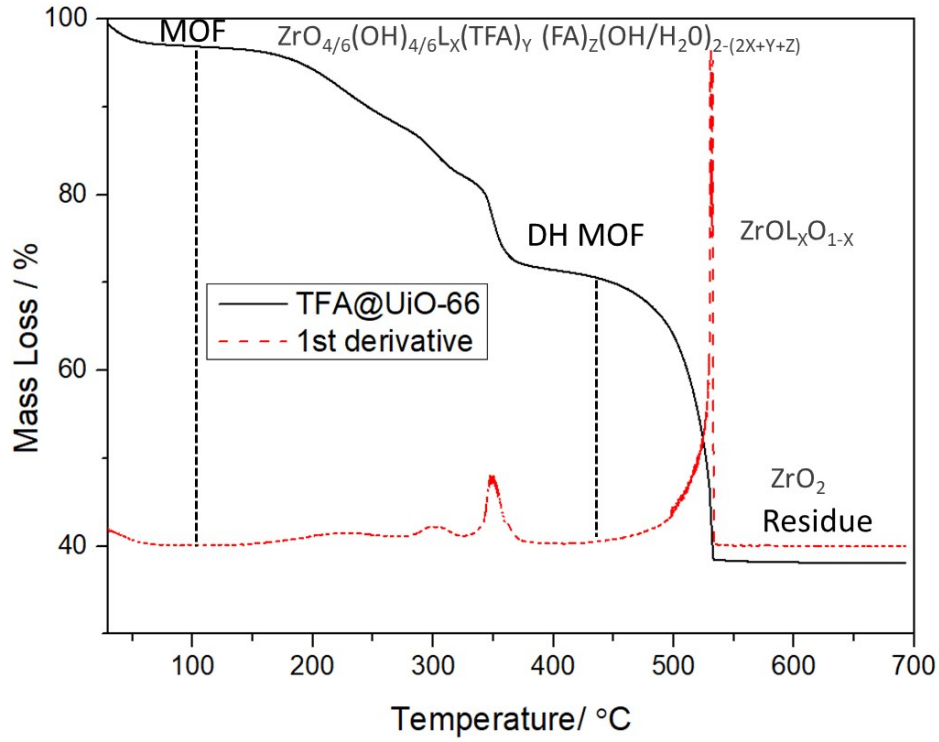

Figure S14: Thermal decomposition profile of TFA@UiO-66 normalizing the start of the decomposition profile to 100%, alongside with its proposed structure.

Due to the clear start of the DH MOF decomposition profile (prior to the decomposition of linkers) and to the presence of DMF molecules (characterized by ^{1}HNMR) that could be paired with defect-compensating OH^- molecules to balance the coordination number of the metals, we have analyzed the thermal decomposition profiles to obtain the number of linkers in the structures based on the mass ration between the DH MOF and the thermal residue (R_{expDH}).[3] It is important to note that while FA and TFA decompose before the DH MOF leading to the $ZrOL_xO_{1-x}$ structure, BA decomposes during the DH MOF, [4] thus leading to the $ZrOL_x(BA)_yO_{1-(x+y/2)}$. Hence, the formula for FA and TFA will be:

$$R_{expDH} = \frac{M_w\,[DH\ MOF]}{M_w\ [Residue]} = \frac{M_w\ [ZrO(L)_xO_{1-x}]}{M_w\ [ZrO_2]}$$

Then,

$$X\ Ligands = \frac{\left(R_{expDH} * M_w\,[\,ZrO_2]\right) - M_w\ [ZrO] - M_w\,[O]}{M_w\,[L] - M_w\,[O]}$$

While for BA it will be

$$R_{expDH} = \frac{M_w\,[DH\ MOF]}{M_w\ [Residue]} = \frac{M_w\ [ZrO(L)_x(BA)_yO_{1-(x+\frac{y}{2})}]}{M_w\ [ZrO_2]}$$

BA is introduced as a function of the linkers using the molar ratios previously determined by ^{1}HNMR,

Then,

$$X\ Ligands = \frac{\left(R_{expDH} * M_w\,[\,ZrO_2]\right) - M_w\ [ZrO] - M_w\,[O]}{M_w\,[L] + NMR * M_w\,[BA] - \left(1 + \frac{NMR}{2}\right) * M_w\,[O]}$$

Once the number of linkers in the structure has been calculated, the number of modulators are obtained by multiplying the number of linker by the mod/L molar ratio determined by ^{1}HNMR.

Then, the number of OH- molecules compensating for the charge arising from the missing linkers is calculated using the charge balance equation.

$$4\ (Charge\ Zr) = \frac{4}{6} * 2\ O + \frac{4}{6} * OH + 2 * X\ Ligand + Y\ Mod1 + Z\ Mod2 + D\ OH$$;

$$D\ OH = 2 - 2 * X\ Ligand - y\ Mod1 - z\ Mod\ 2$$

Then, to calculate the number of DMF and/or H_20 molecules paired to OH^- defect compensating species, the DMF/L molar ratios determined by NMR are multiplied by the number of linkers, thus obtaining the number of DMF molecules in the structures. Those are subtracted to the OH^- molecules to calculate the number of paired OH molecules.

If higher values are obtained for DMF than for OH- molecules, we assume that, despite having activated the samples with Soxhlet (MeOH) and subsequent vacuum at 120°C during 24h, DMF molecules could be obstructed in the pores.

The values of R_{exp} and R_{expDH} are given in **Table S2**, and the composition values obtained by this method in **Tables S3** and **S4**. We calculated the theoretical mass ratio between the calculated structures and their residue to validate the method (R_{theo} and R_{theoDH})

Table S2: Experimental mass ratio between the molecular weight of the MOF (R_{exp}) and the DH MOF (RexpDH) at different decomposition stages and its thermal residue.

Sample	**R_{EXP}**	**R_{EPXDH}**
BA	2.40	2.10
FA	2.28	1.91
TFA	2.53	1.85

Table S3: Composition of modulated UiO-66 $(Zr_6O_6(OH)_6(L)_X(Mod)_y(FA)_z(OH/H_2O)_d$ extracted from the combination of TGA and NMR. Note that all the DMF is compensating for the coordination sphere of Zr6 in FA@UiO-6, for which also water molecules are need to maintain Zr coordination number, while in TFA and BA modulated samples there is a higher DMF content that the needed to compensate the coordination number arising from OH-coordination and thus a part of DMF (DMF-OH) must be obstructed in the pores.

Sample	**L**	**FA**	**MOD (added)**	**OH**	**DMF**	**H_2O**	**ML**	**Total Mod per ML**

BA	4.711	0.843	0.906	0.829	2.537	N/A	1.289	1.357
FA	4.557	1.332	1.332	1.553	1.319	0.234	1.443	0.923
TFA	4.259	0.917	1.800	0.765	2.650	N/A	1.741	1.561

Table S4: Molar per cent of missing linkers, weight per cent of Zr per DH MOF, molecular weight, coordination by linker of modulated and theoretical mass ratios between the calculated structures and their residue UiO-66 $(Zr_6O_6(OH)_6(L)_X(Mod)_y(FA)_z(OH/H_2O)_d$ extracted from the combination of TGA and NMR.

Sample	**%ML**	**Wt% Zr /DH MOF**	**Mw MOF**	**Coordination by L**	**R_{theoDH}**	**R_{theo}**
BA	21.478	47.596	296.3	9.42	2.10	2.49
FA	24.050	53.104	276.9	9.11	1.91	2.22
TFA	29.018	54.248	311.9	8.52	1.85	2.48

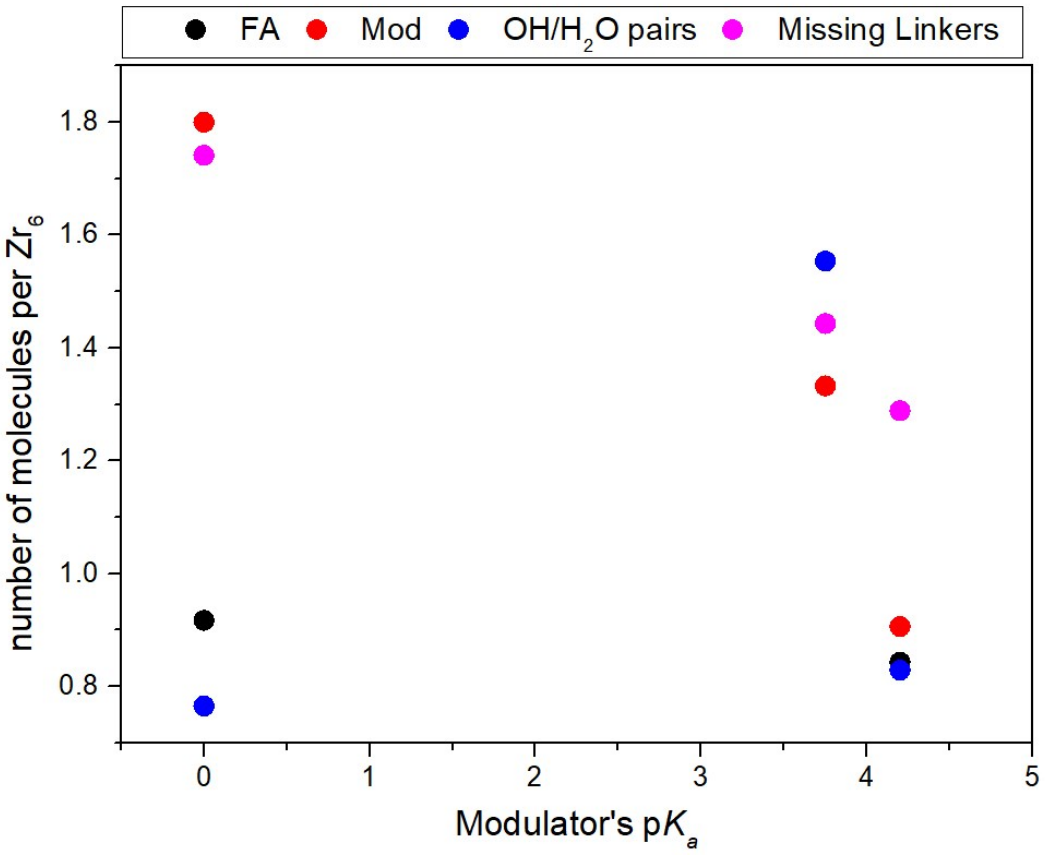

Figure S15: Representation of the modulated MOFs composition as a function of the acidity of the modulator.

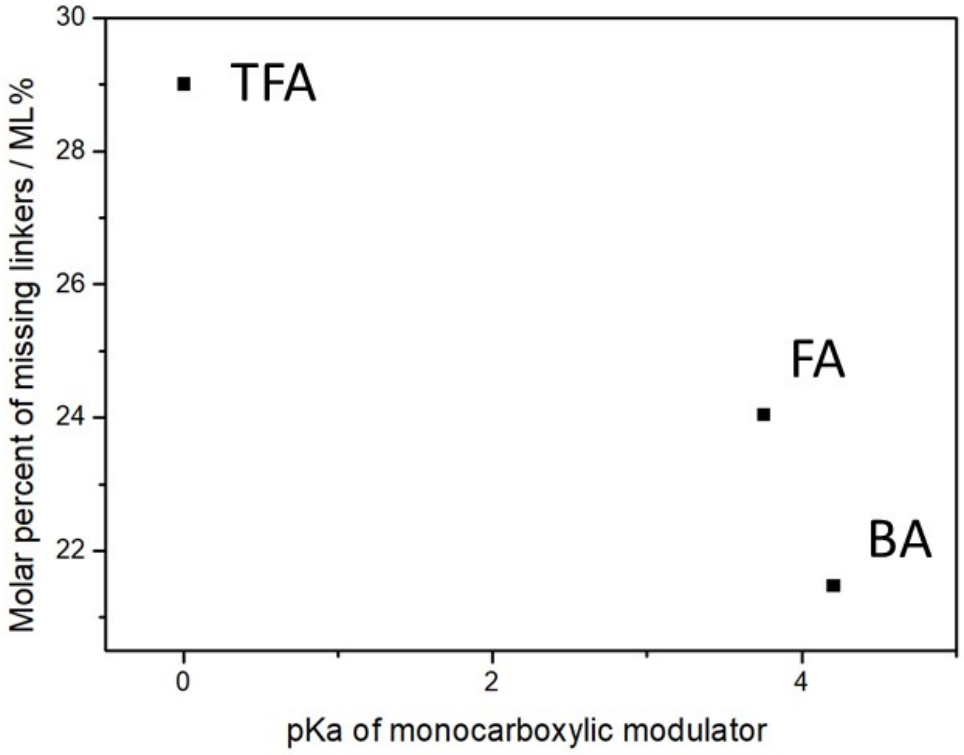

Figure S16: Representation of the relation between the molar per cent of missing linkers and the acidity of the modulator.

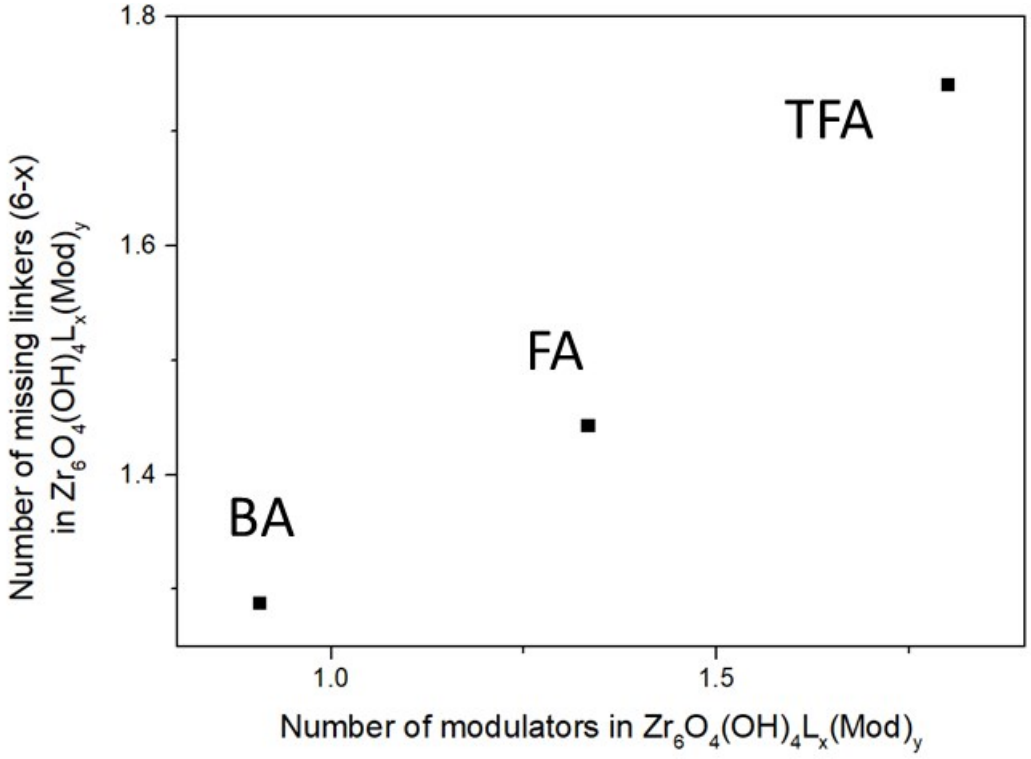

Figure S17: Representation of the relation between the number of modulators and missing linkers in the structure.

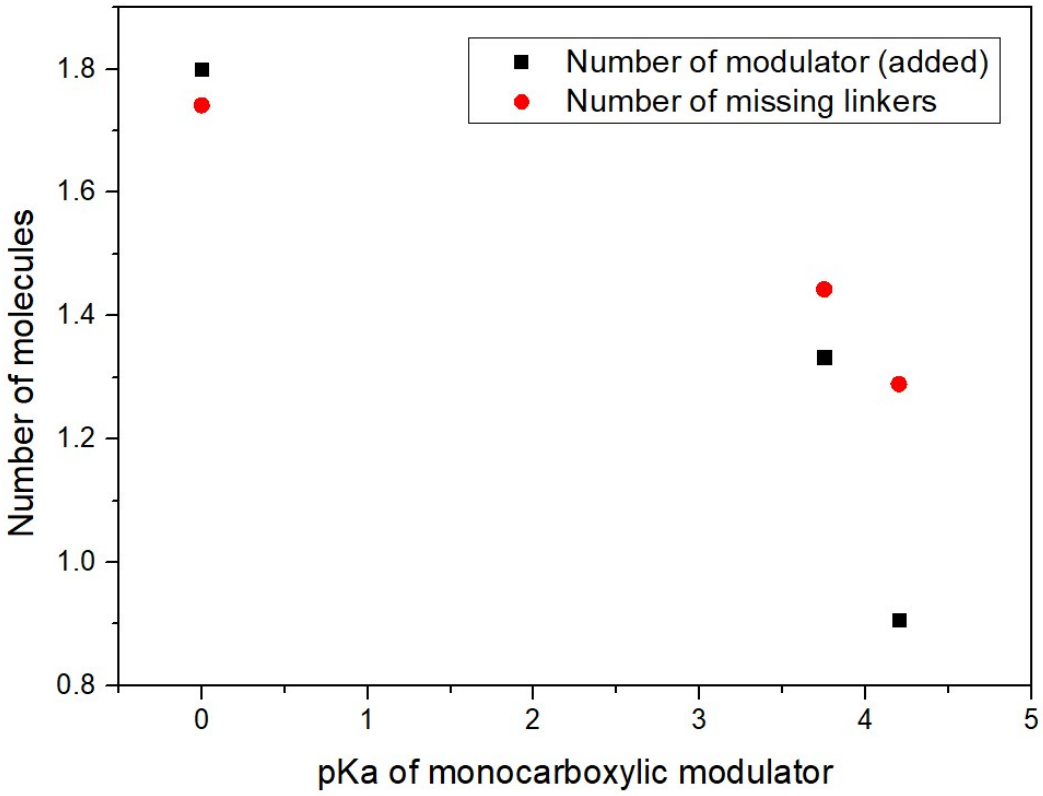

Figure S18: Representation of the relation between the number of missing linkers and modulator, and the acidity of the modulator.

S.3.5. Assessing particle size by SEM.

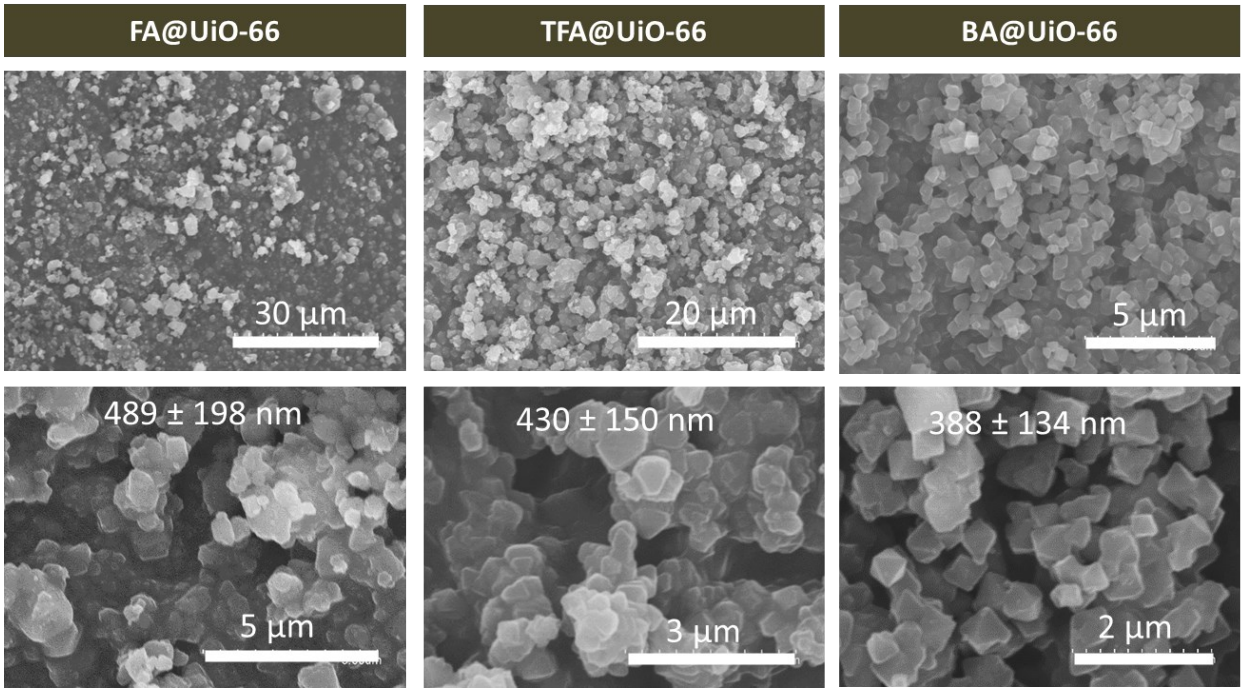

Figure S19: SEM images of modulated UiO-66.

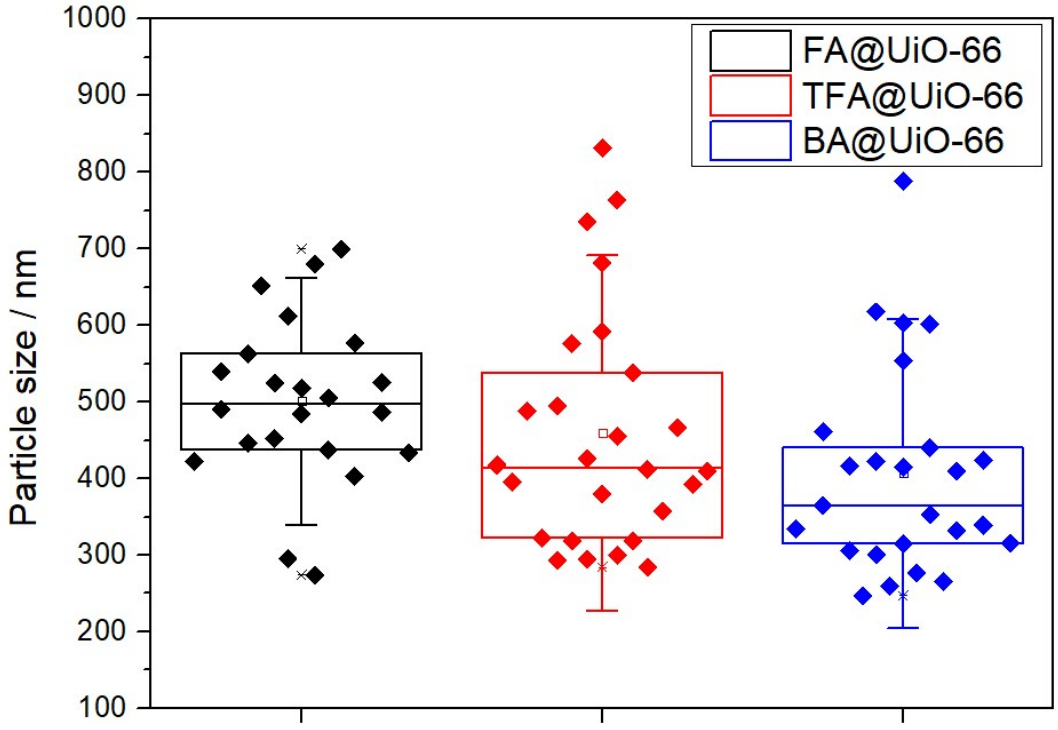

Figure S20: Statistical representation of the analysed particle size of modulated UiO-66. The box chart represents the average ± SD particle size, alongside with the 25% and 75% percentiles for a bin size of 100 nm and particle size count higher than 20.

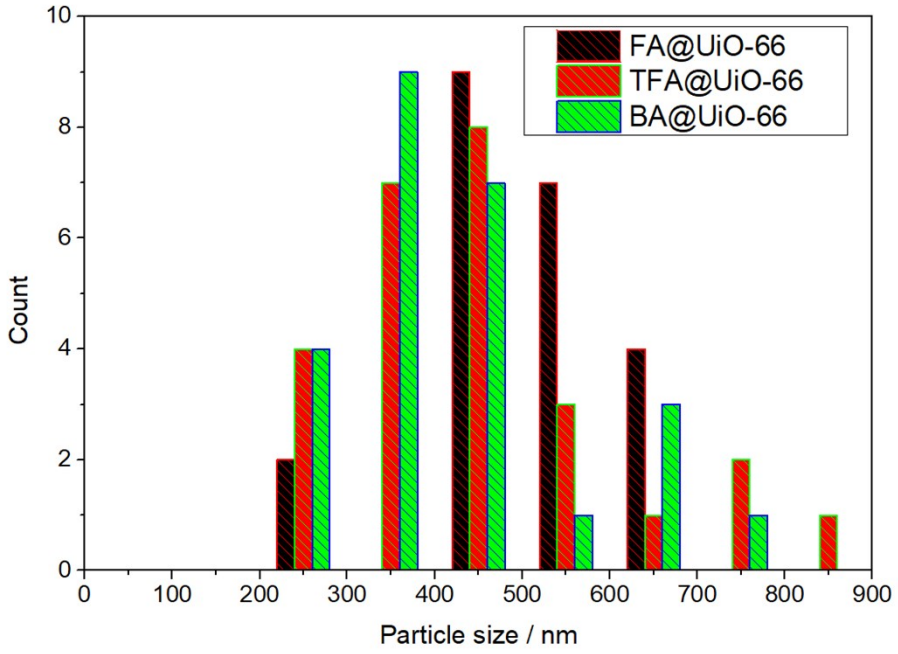

Figure S21: Histogram representation of modulated-UiO-66 particle sizes.

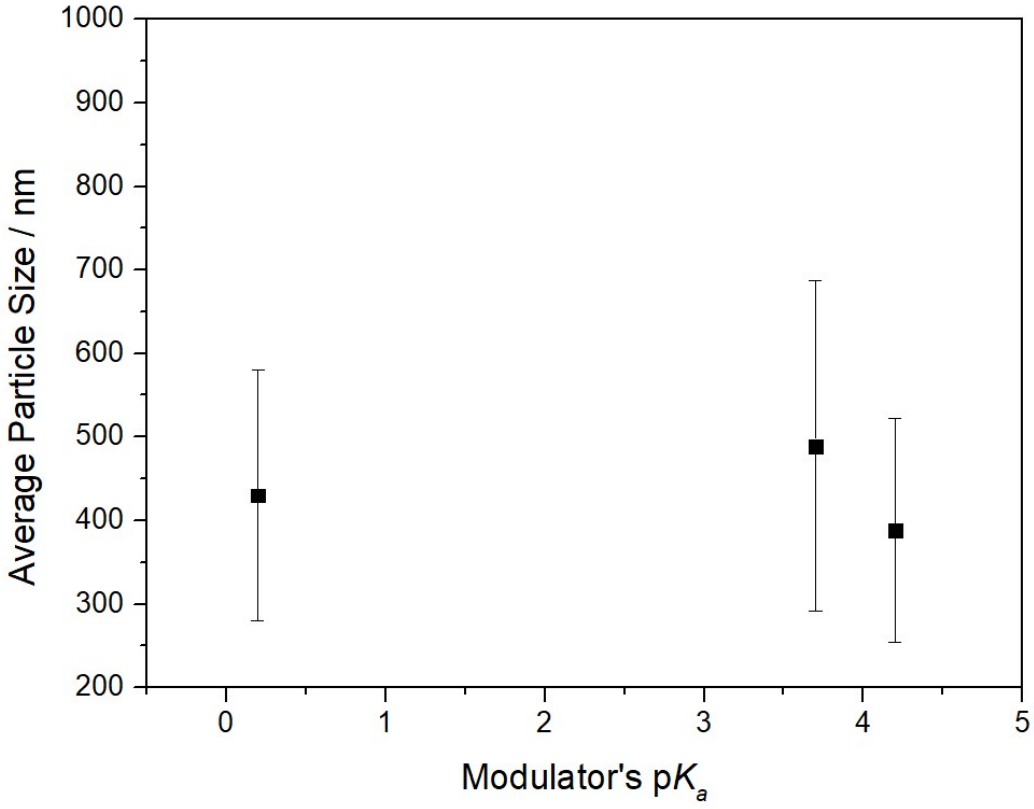

Figure S22: Representation of modulated-UiO-66 particle sizes as a function of the modulator pK_a, showing no relation.

S.3.6. Assessing MOFs porosity by N_2 adsorption and desorption isotherms

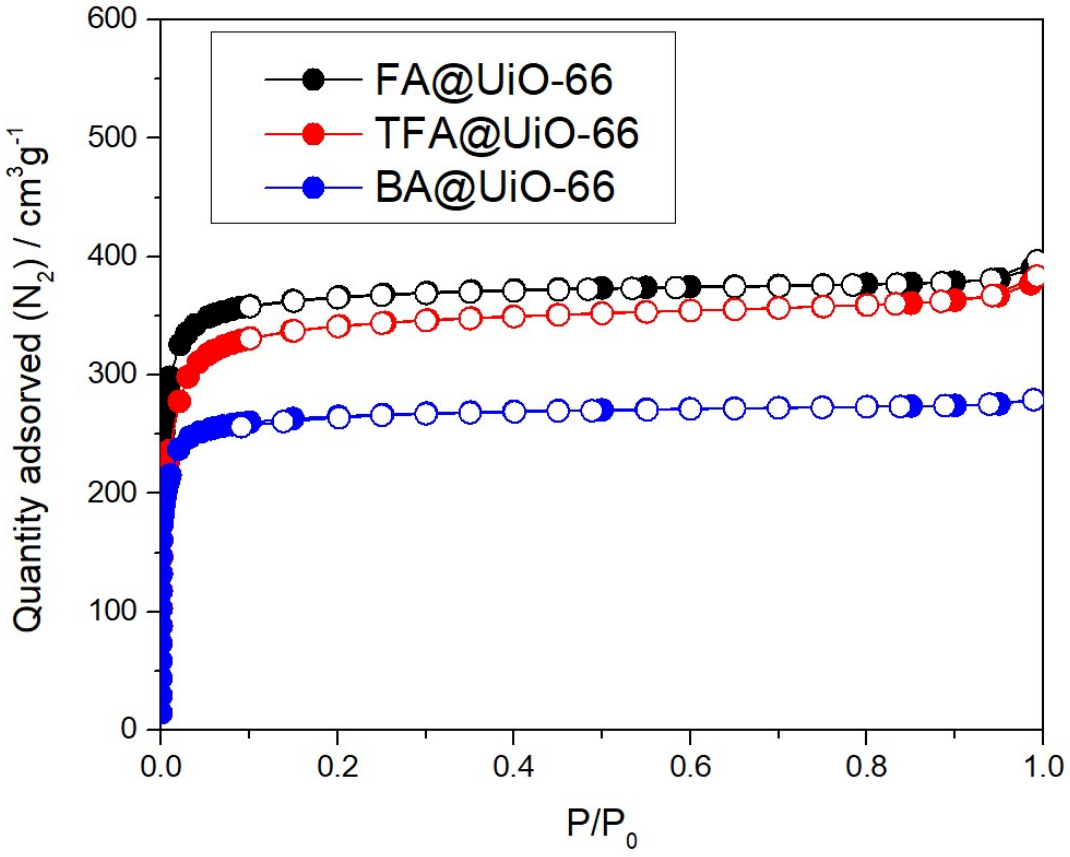

Figure S23: N_2 adsorption and desorption isotherms of modulated UiO-66.

Table S5: Tabulated data extracted from N_2 adsorption and desorption measurements of modulated UiO-66. Note that slightly lower S_{BET} and S_{micro} values are obtained for TFA and BA modulated samples, in great agreement with TGA revealing DMF molecules possibly obstructed in the pores.

Sample	**S_{BET} / S_{MICRO} / S_{EXT}(m^2/g)**	**Micro / Meso pores volume (cm^3/g)**		**Total Pore volume (cm^3/g)**
BA@UiO-66	1042 / 929/113	0.362	0.071	0.433
FA@UiO-66	1393 /1226/167	0.494	0.121	0.615
TFA@UiO-66	1389 / 1165/224	0.431	0.164	0.595

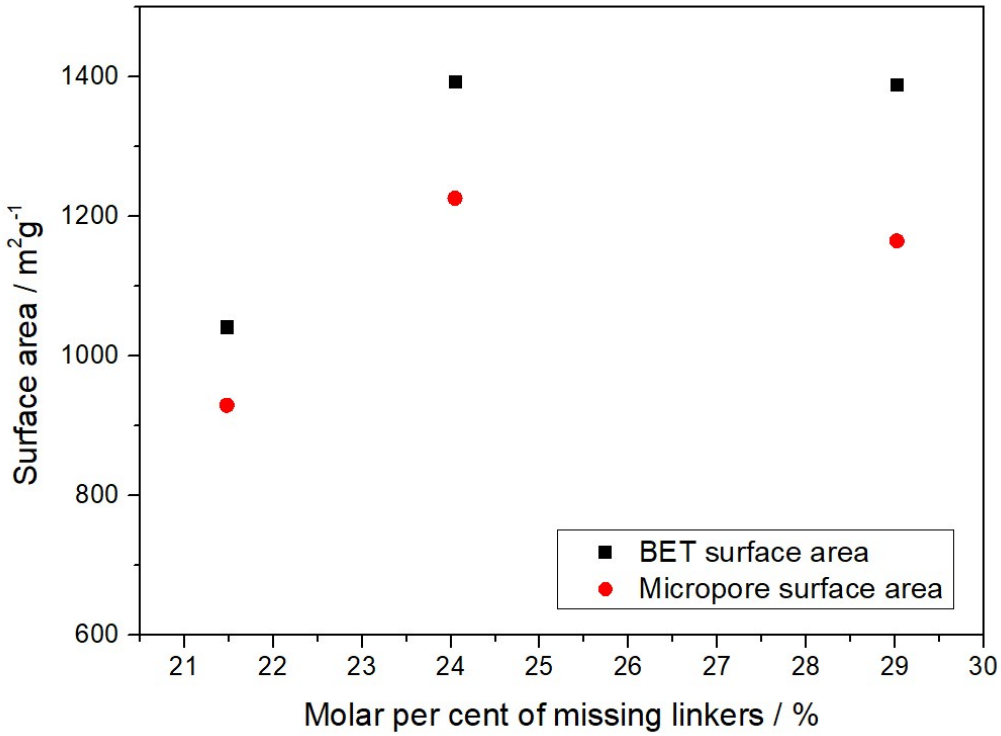

Figure S24: Representation of the relation of the BET and micropore surface area with the molar per cent of missing linkers.

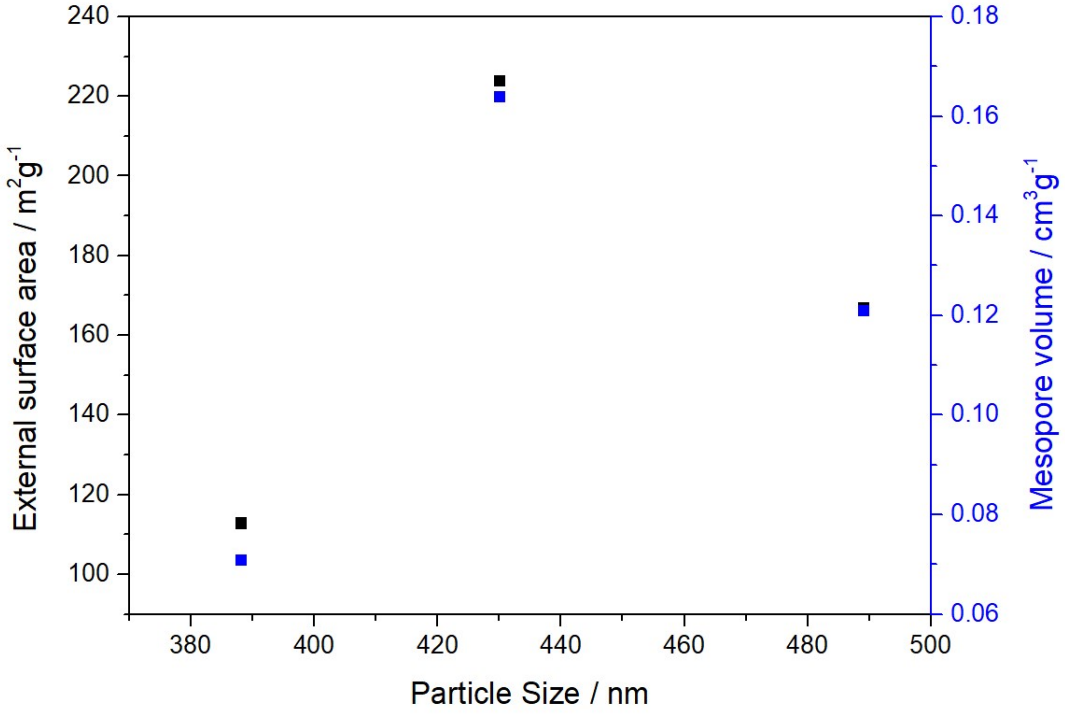

Figure S25: Representation of the relation of the external surface area and mesoporosity with the particle size calculated by SEM, showing no relation.

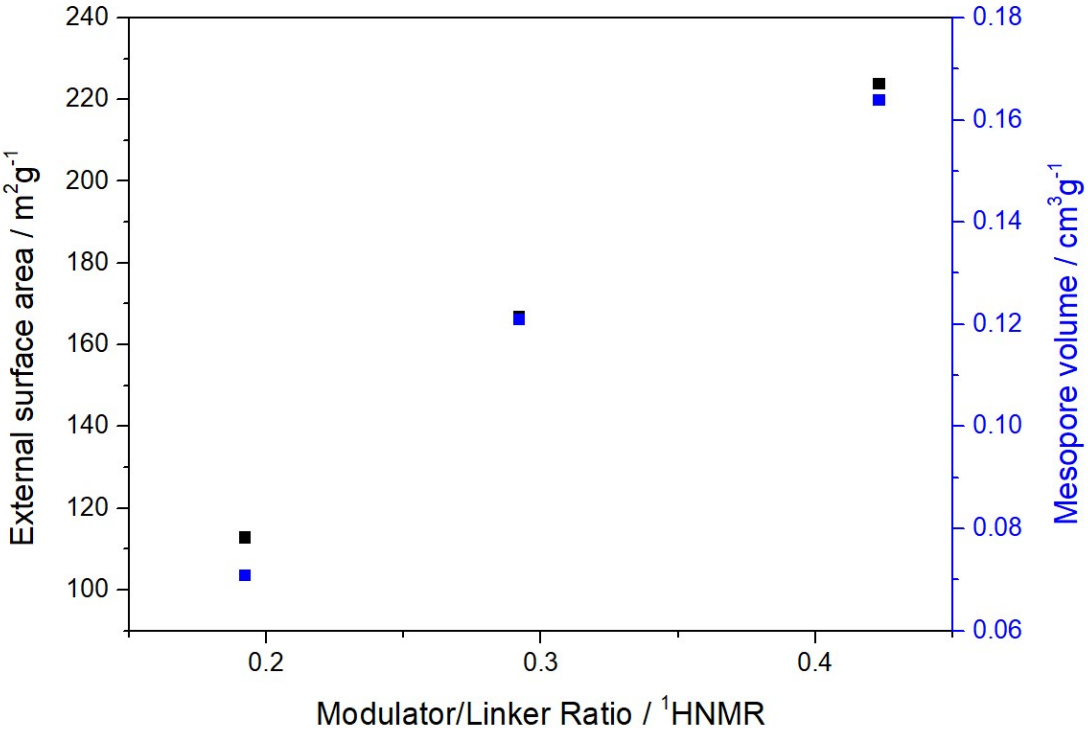

Figure S26: Representation of the relation of the external surface area and mesoporosity with the molar ratio between modulator and linker calculated by NMR.

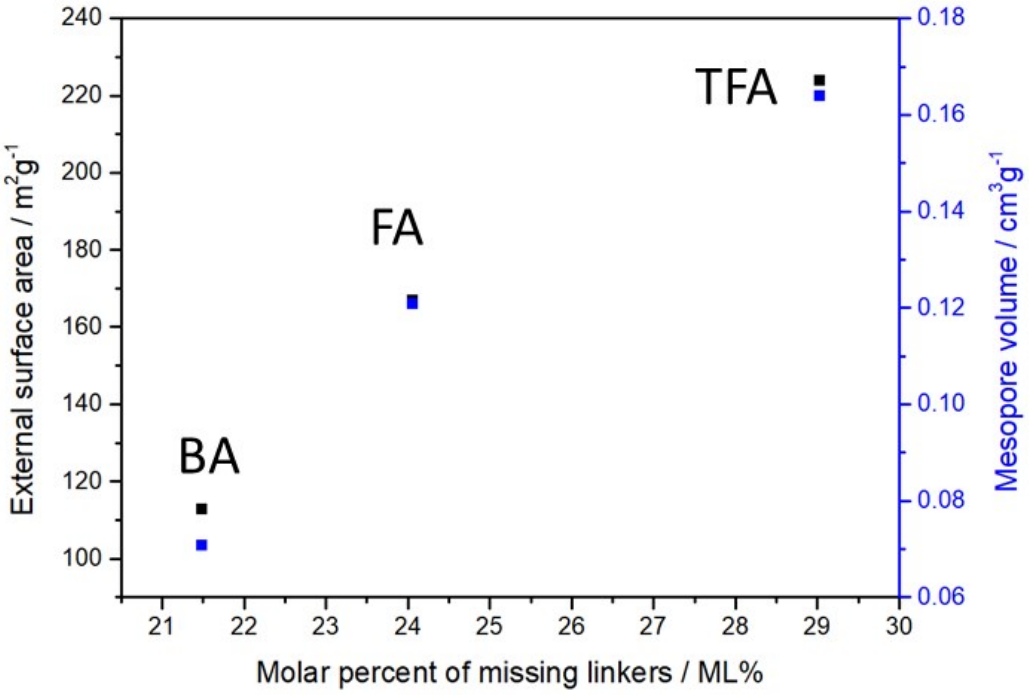

Figure S27: Representation of the relation of the external surface area and mesoporosity with the molar per cent of missing linkers

S.4. Catalytic activity of UiO-66 modulated samples

10 µL of cyclohexene oxide and 10 µL of aniline were dissolved in 0.5 mL of ethanol and let them react at room temperature in the presence of 10 mg of MOF for one day. Sample aliquots were analysed by GC-FID (Gas Chromatography-Flame Ionization Detector.

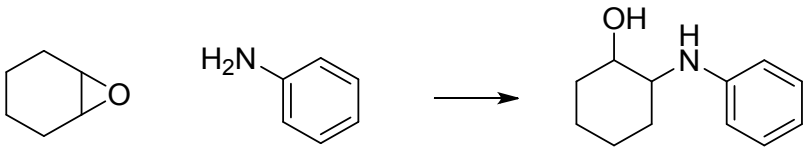

Table S6: Tabulated data of conversion % and selectivity % after 8 h and 24 h of reaction.

Sample	8 h		24 h	
	% conversion	% Selectivity	% conversion	% Selectivity
Blank	1	99	3	99
BA@UiO-66	45	87	69	90
FA@UiO-66	51	87	74	87
TFA@UiO-66	59	86	80	86

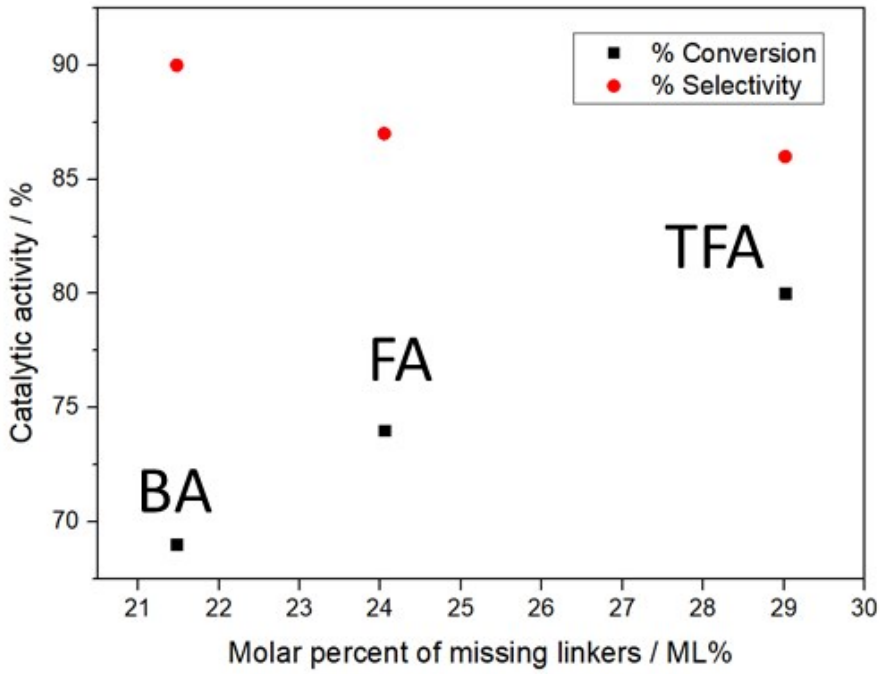

Figure S28: Representation of the relation catalytic conversion and selectivity as a function of the molar per cent of missing linkers.

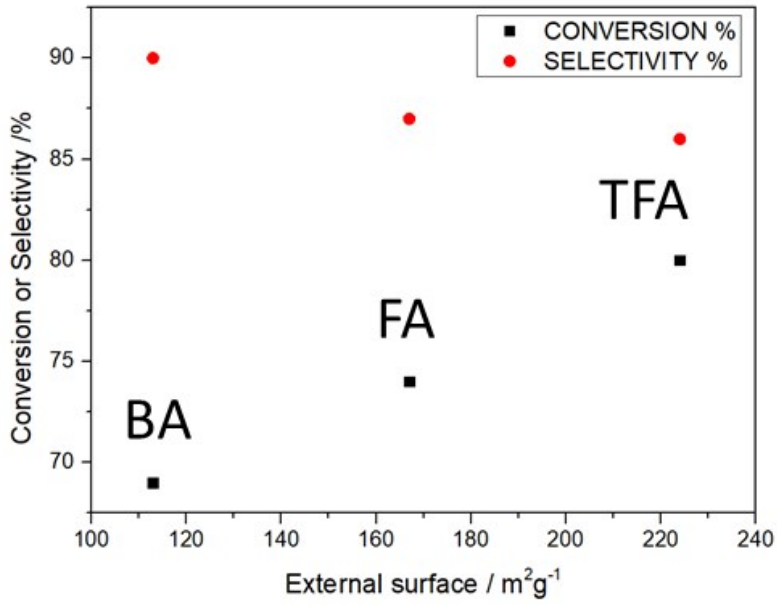

Figure S29: Representation of the relation catalytic conversion and selectivity as a function of the external surface area.

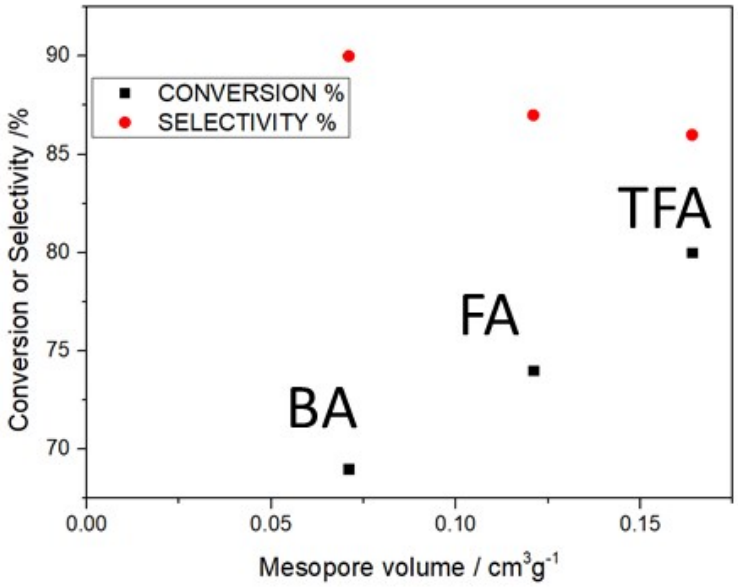

Figure S30: Representation of the relation catalytic conversion and selectivity as a function of the mesopore volume.

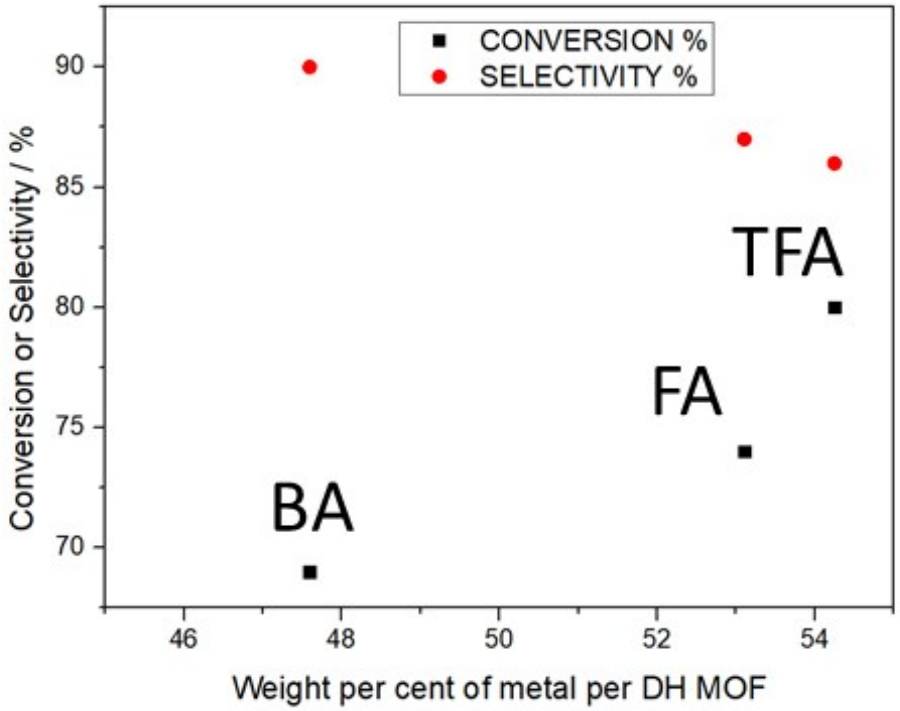

Figure S31: Representation of the relation catalytic conversion and selectivity as a function of the weight per cent of metal per DH MOF.

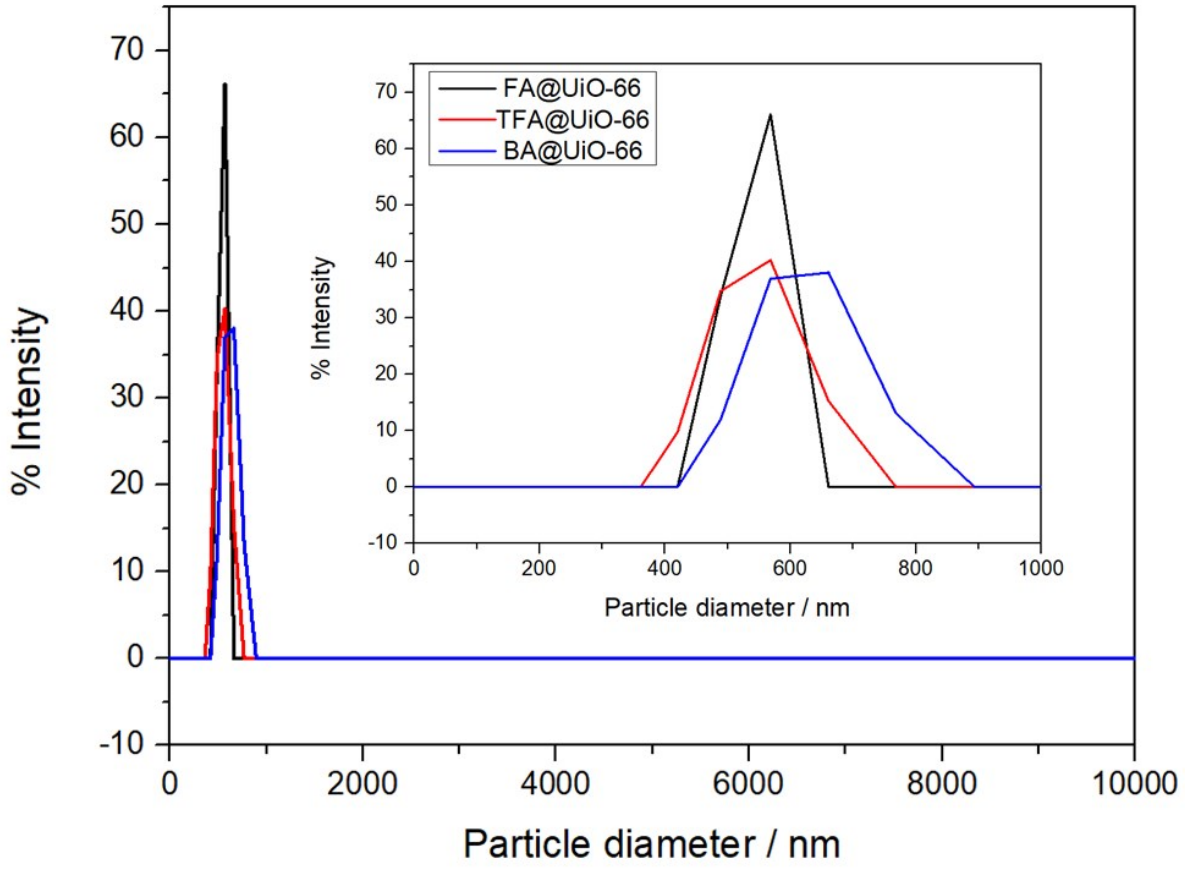

Figure S32: Representation of the polydispersity of the samples in EtOH, showing good dispersion in the catalytic media for all samples.

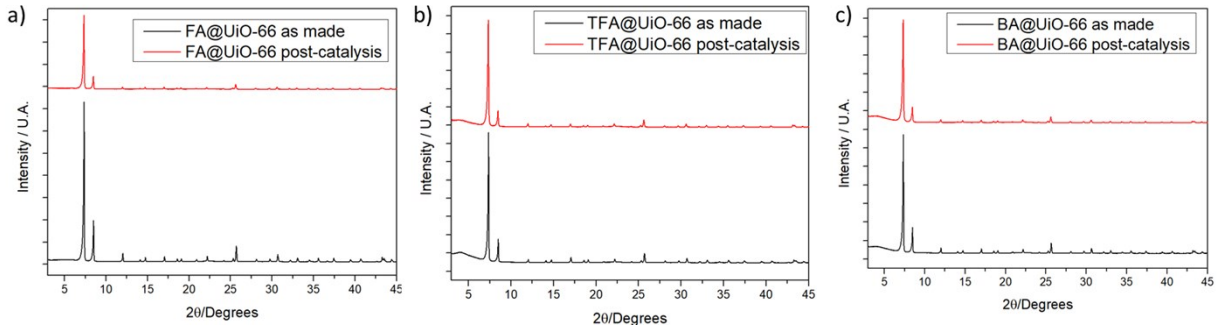

Figure S33: Representation of the PXRD patterns of the samples before and after the catalytic reaction.

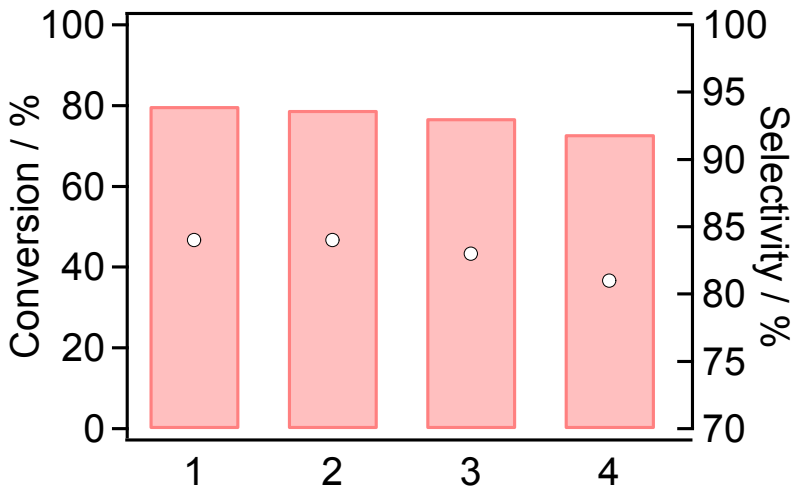

Figure S34: Recycling of UiO -66 (TFA) during 4 reaction runs of ring opening of cyclohexene oxide with aniline in ethanol, showing maintained catalytic activity. Bars represent conversion of the epoxide while dots represent selectivity to amino alcohol. For the recycling test, the spent catalyst was thoroughly washed with ethanol and dried under vacuum before being used in a subsequent cycle.

S.5. References

(1) F. Fauth, I. Peral, C. Popescu, M. Knapp, *Powder Diffr.,* 2013, **28**, 360–370.

(2) G. C. Shearer, S. Chavan, S. Bordiga, S. Svelle, U. Olsbye and K. P. Lillerud, *Chem. Mat*er., 2016, **28**, 3749-3761.

(3) I. A. Lázaro, *Eur. J. Inorg. Chem.*, 2020, **2020**, 4284-4294.

(4) C. Atzori, G. C. Shearer, L. Maschio, B. Civalleri, F. Bonino, C. Lamberti, S. Svelle, K. P. Lillerud and S. Bordiga, *J. Phys. Chem. C*, 2017, **121**, 9312–9324.